Journal Title
XX(X):1–7

DOI: 10.1177/ToBeAssigned
www.sagepub.com/
SAGE

Influence of Employing Laminated Isogrid Configuration on Mechanical Behavior of Grid Structures

Amir Ehsani[1] and Hamid Dalir[1]

Abstract

For a long time, a single grid layer, such as isogrid, have been utilized to strengthen a shell or plate or as an independent structural member for various applications. Laminated grid structures consist of several grid layers, that can have different in-plane orientations or can be made from different materials. Therefore, using laminated configuration instead of conventional grids yields to an extensive variety of configurations with different coupling effects and cost. In the current paper, to evaluate the appropriateness of laminated isogrids, the vibration and stability behaviors of a conventional isogrid are compared with corresponding laminated isogrid plate. The first-order shear deformation plate theory as well as the Ritz theorem is utilized to achieve the critical buckling loads and free vibration frequencies of the plates. The influence of increasing the number of isogrid plies and changing pattern geometries on mechanical behaviors of the laminated isogrid plate are also investigated. The results imply, utilization of the laminated isogrids remarkably enhances the buckling load and free vibration frequency values of the plates.

Keywords

Laminated isogrid, Buckling load, Free Vibration Frequency, Grid Stiffened Structures

Introduction

Grid or lattice structures are extensively employed in abundant structures that for most of them weight is a crucial factor to design and use, such as airplanes, ships, vehicles, and buildings. There are many grid patterns to use in different applications in industries, namely isogrid, orthogrid, and anglegrid, etc. Due to resistance to environmental exposure, low weight and manufacturing expenses, the grids are mostly produced by fiber reinforced composites.

Up to now, majority of investigations have been focused on modeling, prediction of mechanical behavior, manufacturing, and optimization of conventional grid or lattice structures. Several earlier works have been studied free vibration of the stiffened structures employing different methods such as isoparametric finite elements, spline compound strip, etc.[1–8]. In multiple previous studies buckling and post-buckling behaviors of grid stiffened shells and plates have been investigated employing various analytical, numerical and experimental methods such as smeared stiffener, equivalent stiffness, finite element, etc.[9–17]. Ehsani and Rezaeepazhand[18] presented a new class of grid structures which are known as "laminated grid structures". They investigated lamination effects on stiffness and mechanical behavior of grid structures. Ehsani et al.[19,20] studied the influence of the stacking sequence and pattern arrangement on buckling load of laminated composite grid plates and also conducted studies on the buckling load and natural vibration of laminated orthogrid plates. Their results showed that, there are proper stacking sequences, which considerably improves the mechanical behaviors of the grid structures. Ehsani and Dalir[21] investigated the axial buckling load and maximum lateral deformation of laminated and conventional anglegrid plates. They evaluated the effectiveness of using different tip angles along with the various orientation of each anglegrid layer. Ehsani and Dalir[22] studied the effectiveness of using laminated isogrid structures as a trunk floor in automotive industry. They showed employing a suitable laminated grid plate as a stiffener can reduce the lateral deflection of a hypothetical trunk floor.

Despite the diverse studies on conventional grid structures, there has been insufficient focus to date in the literature on the laminated grid structures. Resembling to typical laminated composite structures, laminated grids are composed from multiple grid plies which each grid ply may has different orientation or even different pattern. Figure 1a illustrates a laminated grid that consists of three isogrid plies with (0°/45°/0°) lay-up. Figure 1b shows a conventional isogrid plate with identical thickness to the laminated isogrid.

Among different grid patterns, the isogrid is extensively used in different industries. However, there is no published studies about effects of using laminated isogrid instead of conventional isogrid structures. Therefore, to evaluate this new class of isogrid structures, in the present study, the critical axial and shear buckling loads, and two first free vibration frequencies of the laminated and conventional isogrid structures are obtained using First-order Shear Deformation Plate Theory (FSDT). The influence of increasing the number of isogrid plies on mechanical responses is studied employing several laminated isogrids

[1]Department of Mechanical and Energy Engineering, Purdue School of Engineering and Technology

Corresponding author:
Hamid Dalir, Department of Mechanical and Energy Engineering, Purdue School of Engineering and Technology, Indianapolis, USA
Email: hdalir@purdue.edu

This is the author's manuscript of the article published in final edited form as:
Ehsani, A., & Dalir, H. (2019). Influence of employing laminated isogrid configuration on mechanical behavior of grid structures. Journal of Reinforced Plastics and Composites, 38(16), 777-785. https://doi.org/10.1177/0731684419848046

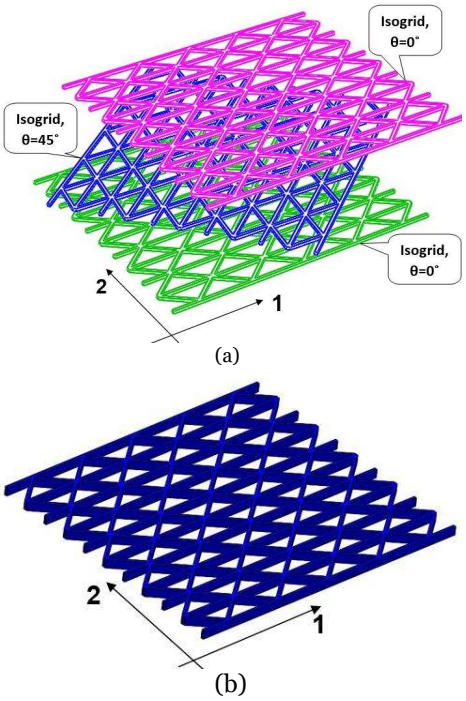

Figure 1. A three-ply isogrid plate (laminated isogrid), with (0°/45°/0°) stacking sequence (a), a conventional isogrid plate with similar total thickness and geometry(b)

with different number of plies. Moreover, to investigate the effects of the pattern's geometry, two different isogrid plates with identical weight and thickness and dissimilar rib's space and width are considered and compared.

Problem Description

Laminated Isogrid Configuration

A rectangular plate of length a, width b, and thickness H, as depicted in Figure 2, is considered in this study. The plate is assumed to be simply supported along all its sides and is under an uniaxial compression or a shear load. The plate is composed of N perfectly bonded composite isogrid plies which are symmetrically stacked related to mid-plane.

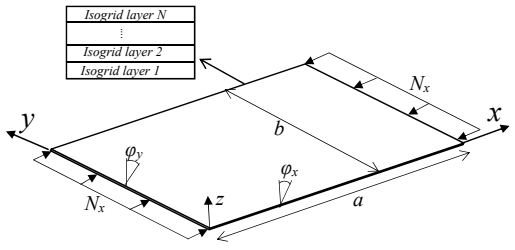

Figure 2. The schematic laminated isogrid plates under uni-axial compressive force

To evaluate the geometry effects on mechanical behavior of the laminated and conventional isogrid plates, two different isogrid geometries are designed for this study. Both have identical weight and thickness. However, the ribs' spaces (d_1, d_2, d_α), ribs' widths (t_1, t_α) and tip angle (α) are dissimilar in geometries. Figure 3 illustrates both geometries. The dimensional parameters are considered according to the following conditions: $(d_1)_1 = 25mm$, $(d_1)_2 = 15mm$, $(d_2)_1 = 37.5mm$, $(d_2)_2 = 75mm$, $\alpha_1 = 33°$, $\alpha_2 = 11°$, $(t_1)_1 = (t_\alpha)_1$ and $(t_1)_2 = (t_\alpha)_2$.

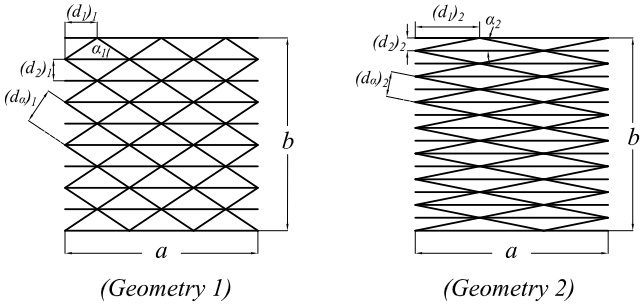

Figure 3. Two considered geometry configurations

In a laminated isogrid, each isogrid ply may have a different orientation related to the plate's sides. Figure 4 depicts a specially isogrid and a generally isogrid plate, that is oriented at an angle θ with respect to the x-axis

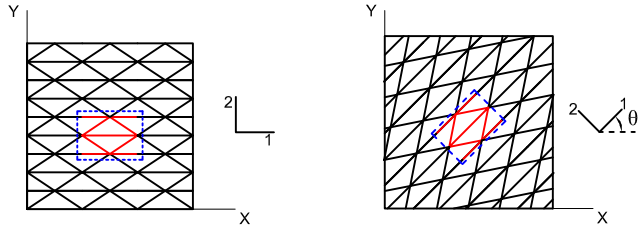

Figure 4. A specially isogrid plate ($\theta = 0°$) (left). A generally isogrid plate which is oriented at an angle $\theta°$ with respect to the x-axis (right)

In addition to the mentioned geometries, two cases of isogrid structures are studied in the present work. The first case is related to laminated isogrids. This case consists of five laminated isogrid plates with $(\pm\theta)_{ns}$ configuration, where $n = 1, 2, ..., 5$. The subscripts "s" and "n" indicate symmetry and number of the $(\pm\theta)$ in the half of the plate thickness, respectively. For example, if $n = 1$, the laminated isogrid will consist of four plies.
The second case is a single conventional isogrid plate. Its geometry, dimensions, weight, and thickness are analogous to the laminated isogrids. It is worth noting that the total thickness is constant for all defined cases even have various number of the plies. Thus, for the overall thickness, H, each ply thickness can be achieved by $H = N \times h$, where N and h are the number of plies and the plies thickness, respectively. Table 1 expresses the cases and their configurations.

Case No.	Type of isogrid structure	Lay-up	Stacking sequence	Number of layers (N)	Each grid layer thickness
1	Laminated isogrid	Sub-laminate	$(\pm\theta)_{ns}$	4n, n=1, 2,...,5	h=H/4n
2	Conventional isogrid	isogrid	(θ)	1	h=H

Table 1. Specifications of the defined cases (laminated isogrids and conventional isogrid)

It is assumed that, T300/5208 Carbon-Epoxy material with the following elastic properties is used to fabricate the isogrid structures: $E_1 = 162 \times 10^9$ Pa, $E_2 = 14.9 \times 10^9$ Pa, $\nu_{12} = 0.283$, $G_{12} = 5.7 \times 10^9$ Pa,$G_{13} = 5.7 \times 10^9$ Pa,

$G_{23} = 5.4 \times 10^9$ Pa, and $\rho = 1583\ kg/m^3$. Where E_1 and E_2 are the composite modulus in fiber direction and transverse to the fiber direction, respectively. G_{12}, ν_{12} and ρ are shear modules, Poisson's ratio and density of the employed composite material, respectively. G_{13}, and G_{23} are the out-of-plane shear modules of assumed material.[23]

Constitutive Equations

In this study, the First-order Shear Deformation Plate Theory (FSDT) together with Ritz theorem is employed to achieve the axial and shear buckling loads as well as free vibration frequencies of the isogrid plates. According to FSDT, the displacement field for a plate are calculated as:

$$u = u_0(x,y) + z\phi_x(x,y) \quad (1)$$
$$v = v_0(x,y) + z\phi_y(x,y) \quad (2)$$
$$w = w(x,y) \quad (3)$$

Where u, v and w are the displacements in the x, y and z directions. The subscript "0" implies the mid-plane deflection. The ϕ_y and ϕ_x represent rotation angles of transverse normal in the mid-surface along x and y directions (see Figure 2). A grid layer has the directional properties which is engendered by the ribs' position and geometry. In this way, similar to a composite lamina, the stress-strain equation for an isogrid ply can be given by:

$$\begin{bmatrix}\sigma_x\\ \sigma_y\\ \tau_{xy}\\ \tau_{yz}\\ \tau_{xz}\end{bmatrix} = \begin{bmatrix}\overline{Q}_{11} & \overline{Q}_{12} & \overline{Q}_{16} & 0 & 0\\ \overline{Q}_{12} & \overline{Q}_{22} & \overline{Q}_{26} & 0 & 0\\ \overline{Q}_{16} & \overline{Q}_{26} & \overline{Q}_{66} & 0 & 0\\ 0 & 0 & 0 & \overline{Q}_{44} & \overline{Q}_{45}\\ 0 & 0 & 0 & \overline{Q}_{45} & \overline{Q}_{55}\end{bmatrix}\begin{bmatrix}\varepsilon_x\\ \varepsilon_y\\ \gamma_{xy}\\ \gamma_{yz}\\ \gamma_{xz}\end{bmatrix} \quad (4)$$

Where the elements of the strain matrix can be expressed as the following forms[18]:

$$\begin{bmatrix}\varepsilon_x\\ \varepsilon_y\\ \gamma_{xy}\\ \gamma_{yz}\\ \gamma_{xz}\end{bmatrix} = \begin{bmatrix}u_{0,x}\\ v_{0,y}\\ u_{0,y}+v_{0,x}\\ \phi_y + w_{,y}\\ \phi_x + w_{,x}\end{bmatrix} + z\begin{bmatrix}\phi_{x,x}\\ \phi_{y,y}\\ \phi_{x,y}+\phi_{y,x}\\ 0\\ 0\end{bmatrix} \quad (5)$$

The $[\overline{Q}]$ is the transformed reduced stiffness matrix and can be given by:

$$[\overline{Q}] = [T]^{-1}[Q][T]^{-T} \quad (6)$$

Where $[T]$ and $[Q]$ are the transformation and reduced stiffness matrices[24].
Depending on the isogrid geometry, the elements of reduced stiffness matrix can be achieved using the following equations[19,25]:

$$Q_{11} = \frac{E_1 t_1}{d_1} + \frac{2E_1 t_\alpha}{d_\alpha}\cos^4\theta + \frac{8G_{12}t_\alpha}{d_\alpha}\cos^2\alpha\sin^2\alpha \quad (7)$$
$$Q_{12} = Q_{21} = 2(\frac{E_1 t_\alpha}{d_\alpha} - \frac{4G_{12}t_\alpha}{d_\alpha})\cos^2\alpha\sin^2\alpha \quad (8)$$
$$Q_{22} = \frac{2E_1 t_\alpha}{d_\alpha}\sin^4\alpha + \frac{8G_{12}t_\alpha}{d_\alpha}\cos^2\alpha\sin^2\alpha \quad (9)$$
$$Q_{44} = G_{23}(\frac{2b_\alpha}{d_\alpha}\sin^2\alpha) \quad (10)$$
$$Q_{55} = G_{13}(\frac{b_1}{d_1} + \frac{2b_\alpha}{d_\alpha}\cos^2\alpha) \quad (11)$$

$$Q_{66} = \frac{G_{12}t_1}{d_1} + \frac{2E_1 t_\alpha}{d_\alpha}\cos^2\alpha\sin^2\alpha + \frac{2G_{12}t_\alpha}{d_\alpha}(\cos^2\alpha - \sin^2\alpha)^2 \quad (12)$$

Where t_1 and t_α are the width of the horizontal and diagonal ribs, respectively. The d_1, d_2, and d_α are the dimensional parameters (See Figure 3).
The Ritz method is used to obtain the shear and axial buckling loads and free vibration frequencies of the grid plates. Therefore, the total potential energy of the plate is calculated by the following equation:

$$\pi = U - V \quad (13)$$

Where U is the strain energy and V is loss in the potential energy and considering FSDT for a laminated plate, U and V can be given by[26,27]:

$$U = \frac{1}{2}\int_0^a\int_0^b (D_{11}(\frac{\partial\phi_x}{\partial x})^2 + D_{22}(\frac{\partial\phi_y}{\partial y})^2 + 2D_{12}\frac{\partial\phi_y}{\partial y}\frac{\partial\phi_x}{\partial x} + D_{66}(\frac{\partial\phi_y}{\partial x} + \frac{\partial\phi_x}{\partial y})^2 + 2D_{16}\frac{\partial\phi_x}{\partial x}(\frac{\partial\phi_y}{\partial x} + \frac{\partial\phi_x}{\partial y}) + 2D_{26}\frac{\partial\phi_y}{\partial y}(\frac{\partial\phi_y}{\partial x} + \frac{\partial\phi_x}{\partial y}) + A_{44}(\phi_y^2 + 2\phi_y\frac{\partial w}{\partial y} + (\frac{\partial w}{\partial y})^2 + A_{55}(\phi_x^2 + 2\phi_x\frac{\partial w}{\partial x} + (\frac{\partial w}{\partial x})^2 + 2A_{45}\phi_x\phi_y + \phi_x\frac{\partial w}{\partial y} + \phi_y\frac{\partial w}{\partial x} + \frac{\partial w}{\partial y}\frac{\partial w}{\partial x})dxdy \quad (14)$$

$$V = \frac{1}{2}\int_0^a\int_0^b (N_x(\frac{\partial w}{\partial x})^2 + N_y(\frac{\partial w}{\partial y})^2 + 2N_{xy}(\frac{\partial w}{\partial x}\frac{\partial w}{\partial y}) + \frac{h^2}{12}(N_x((\frac{\partial\phi_x}{\partial x})^2 + (\frac{\partial\phi_y}{\partial x})^2) + N_y((\frac{\partial\phi_x}{\partial y})^2 + (\frac{\partial\phi_y}{\partial y})^2) + 2N_{xy}(\frac{\partial\phi_x}{\partial x}\frac{\partial\phi_x}{\partial y} + \frac{\partial\phi_y}{\partial y}\frac{\partial\phi_y}{\partial x})dxdy \quad (15)$$

In the above equation A_{ij} are extensional and D_{ij} are bending stiffness matrix elements of the laminated isogrid plates and are achieved using following equations[24]:

$$A_{ij}, D_{ij} = \sum_{k=1}^{N}(\overline{Q}_{ij})_k[(z_k - z_{k-1}), \frac{1}{3}(z_k^3 - z_{k-1}^3)], \quad i = j = 1,2,4,5,6 \quad (16)$$

Where k is the ply number, z_k is the distance of k^{th} ply from the mid-plane, and N is the number of the isogrid plies in laminated isogrids.
In the current study, it is assumed that, the plates are simply supported along all edges. The trigonometric functions which satisfy the geometrical boundary conditions for Equations (1, 2, 3) can be expressed as:

$$w(x,y) = \sum_{m=1}^{M}\sum_{n=1}^{N} W_{mn}\sin(\frac{m\pi}{a}x)\sin(\frac{n\pi}{b}y) \quad (17)$$

$$\phi_x(x,y) = \sum_{m=1}^{M}\sum_{n=1}^{N} R_{mn}\cos(\frac{m\pi}{a}x)\sin(\frac{n\pi}{b}y) \quad (18)$$

$$\phi_y(x,y) = \sum_{m=1}^{M}\sum_{n=1}^{N} S_{mn}\sin(\frac{m\pi}{a}x)\cos(\frac{n\pi}{b}y) \quad (19)$$

Where W_{mn}, R_{mn} and S_{mn} are constant coefficients. Performing a minimization operation of the total potential energy (Equation 13) with respect to the constant coefficients, an eigenvalue equation is obtained:

$$([K]-\lambda[K_G])\tilde{d}=0 \quad (20)$$

Where $[K]$ and $[K_G]$ are the elastic and geometric stiffness matrices, and $\tilde{d}$ is the vector of coefficients (W_{mn}, R_{mn} and S_{mn}) that can be presented as below[18]:

$$\tilde{d} = \begin{Bmatrix} W_{mn} \\ R_{mn} \\ S_{mn} \end{Bmatrix} \quad (21)$$

Achieving the λ from Equation (20), the buckling loads can be calculated.
To calculate the free vibration frequencies, the energy function of the plate's vibration based on FSDT can be presented as[18]:

$$\pi = U - T_{max} \quad (22)$$

In the above equation, T_{max} is the maximum kinetic energy of the plate and can be obtained by[28]:

$$T_{max} = \frac{\omega^2}{2}\int_0^a\int_0^b(\rho H w^2 + \frac{1}{12}\rho H^3(\phi^2 x + \phi^2 y))dxdy \quad (23)$$

Similar to calculation the buckling loads, minimizing of Equation (22) with respect to the constant coefficients, results in an eigenvalue equation as below:

$$([K]-\omega^2[M])\tilde{d}=0 \quad (24)$$

Where $[M]$ and ω are consistent mass matrix and free vibration frequency, respectively.

Results and Discussion

In the current section the analytical results for axial and shear buckling loads and also first and second free vibration frequencies are presented. Results are obtained for the two defined geometries (see Figure 3) and the two considered cases (see Table 1). The results are represented in non-dimensional form. The non-dimensional critical buckling loads are obtained using $\overline{N} = (N_{cr}b^2)/(E_1H^3)$ and non-dimensional frequencies are defined as $\overline{\omega} = (\frac{\omega b^2}{\pi^2})\sqrt{(\rho/D_{11})}$. To investigate the influence of layer's orientation, θ, on the buckling loads and free vibration frequencies, the layer's orientation has been varied from 0° to 90°. Due to the proximity of values, the corresponding graphs for $n = 2$–4 are not graphically shown in the following figures.
Figure 5 depicts the first non-dimensional axial buckling load for the defined geometries and cases versus layer's orientation, θ. Extracting the maximum values from Figure 5 for each case and geometry, result in Figure 6.

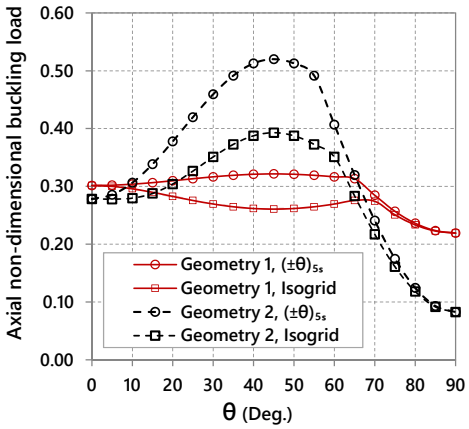

Figure 5. First non-dimensional axial buckling load, $\overline{N_{xcr}}$ for the defined geometries and cases at different layer's orientation, θ

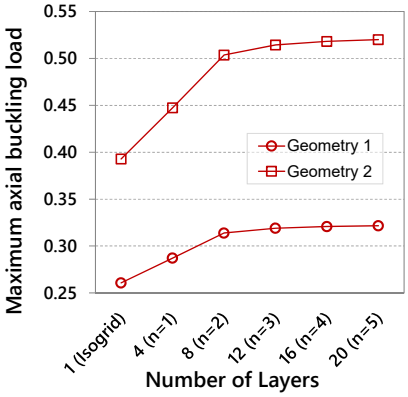

Figure 6. Maximum first axial buckling load for the two defined geometries versus number of layers

Several crucial points can be comprehended from these later figures. Firstly, as can be seen in Figure 5, in both geometries the critical buckling loads' values of laminated isogrid plates are more than the corresponding conventional plates. For example, for Geometry 1 at $\theta = 45°$, the first axial buckling load of the laminated isogrid is about 23% more than corresponding conventional isogrid. Similarly, this value is about 33% for Geometry 2. This point indicates the importance of using laminated isogrid instead of conventional isogrids in various applications.
Secondly, maximum value of the first axial buckling loads

is achieved at $\theta = 45°$. Therefore, the applied orientation of an isogrid layer (whether conventional or in the laminated isogrid) can considerably affect the stability of a structure. For instance, consider the conventional isogrid which is made by Geometry 2. As can be seen, the buckling load value for generally isogrid at $\theta = 45°$ is about 39% more than specially isogrid at $\theta = 0°$ and 3.87 times the specially isogrid at $\theta = 90°$.
Thirdly, despite the fact that, the two defined geometries have identical weight and thickness, but the buckling load values of Geometry 2 is significantly more than corresponding ones from Geometry 1. It can be concluded that the design of an isogrid regardless of weight or thickness plays an important role on buckling behavior of an isogrid plate.
Fourthly, according to Figure 6, for constant weight and thickness, the buckling load has a clear direct relationship with number of layers. Increasing the number of isogrid layers, increases the buckling load of the panel. However, for $n \geq 2$ ($N \geq 8$) the buckling loads yield to a final value and are not substantially affected by increasing the number of isogrid layers. Thus, increasing the number of layers for $N \geq 8$ will not be an affordable choice to improve the stability of a laminated isogrid structure.

Figure 7 illustrates the non-dimensional critical shear buckling loads for the defined geometries and cases. Similar to axial buckling loads, the laminated isogrids decisively have greater values than conventional isogrids. At $\theta = 45°$ the shear buckling load of the geometries 1 and 2 laminated grids, are 36% and 56% more than corresponding conventional isogrids, respectively. Moreover, despite the limited areas, the laminated isogrid which is made by Geometry 2 reaches to the greater load values than Geometry 1. However, for conventional isogrid, Geometry 2 shows no superiority over Geometry 1. Figure 8 shows the maximum shear buckling loads for conventional and laminated isogrid cases. As can be seen, for both geometries between $N = 1$ to 8 the shear buckling load increases drastically. After $n = 2$ ($N = 8$) the load growth is reduced and the graph moves toward a specific value. Therefore, similar to axial buckling load, after $n = 2$, increasing the number of layers has no considerable effect on shear buckling load.

Figure 9 shows the first non-dimensional free vibration frequencies for the defined geometries and cases. As can be seen, in contrast with the buckling load graphs, Geometry 1 cases (laminated and conventional) have an overwhelming advantage over Geometry 2 and their free vibration frequency values are completely more than corresponding ones. Therefore, in addition to the weight, thickness and material, the isogrid design has significant impact on the free vibration frequencies of isogrid structures.

Moreover, the figure illustrates, for Geometry 1 at $\theta = 45°$ the frequency value is about 15% more than corresponding value of conventional isogrid . Similarly, for Geometry 2 this value is about 12.5%. Considering the both geometries, it can be concluded that the laminated isogrids effectively boost up the vibratory behavior of the structure.
Figure 10 depicts the free vibration frequency values at $\theta = 45°$ for different number of layers. Similar to the buckling loads, this value dramatically increases with increasing the number of layers up to $n = 2$ ($N = 8$) and then its growth

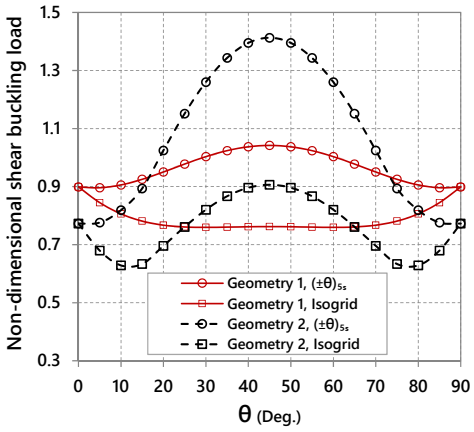

Figure 7. First non-dimensional shear buckling load for the defined geometries and cases, $\overline{N}_{xy}$ at different layer's orientation, θ

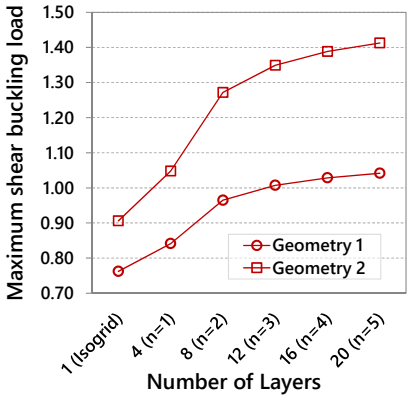

Figure 8. Maximum first shear buckling load for the two defined geometries versus number of layers

suddenly decreases. This manner is common in different analysis (stability and vibration) and also in both geometries.

Figure 11 illustrates the second free vibration frequencies for the defined geometries and cases at different layer's orientation, θ.

As can be seen, similar to the Figure 9, Geometry 1 frequency values are completely over the corresponding values of Geometry 2. Therefore, despite the identical weight and thickness, the geometry is a crucial parameter to evaluate the vibration responses of an isogrid structure. Moreover, the figure shows, for Geometry 1 at $\theta = 45°$ the frequency value is about 21.5% more than corresponding value of conventional isogrid . Similarly, for Geometry 2 this value is about 20%.
Figure 12 depicts the second free vibration frequencies at $\theta = 45°$ for different cases. Similar to the previous figures, two distinguished phases can be seen in the graphs. First, a rapid growth in frequency value along with increasing the number of layers and second tending toward a constant value despite the increase of number of layers.

Conclusion

The current paper investigates the buckling load and natural frequencies of laminated and conventional isogrid structures with constant weight and thickness. Therefore, two different geometries and several laminated isogrids with various

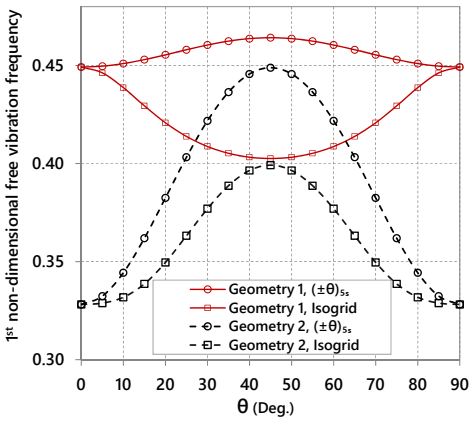

Figure 9. First non-dimensional free vibration frequency, $\overline{\omega}_1$, for the defined geometries and cases

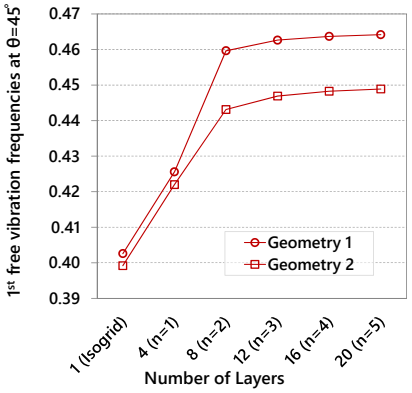

Figure 10. First free vibration frequencies at $\theta = 45^\circ$ for the two defined geometries versus number of layers

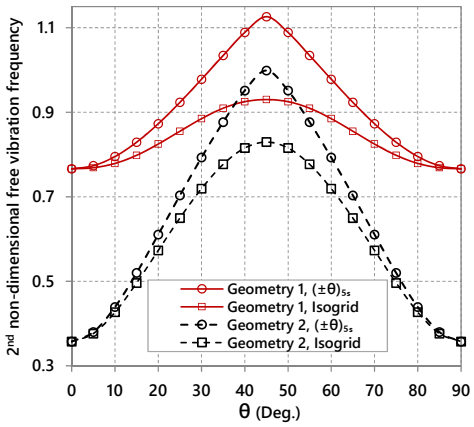

Figure 11. Second non-dimensional free vibration frequency, $\overline{\omega}_2$, for the defined geometries and cases

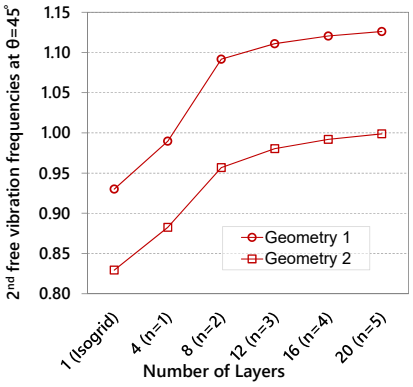

Figure 12. Second free vibration frequencies at $\theta = 45^\circ$ for the two defined geometries versus number of layers

number of layers and identical weight and thickness are considered. The axial and shear buckling loads along with first and second free vibration frequencies are obtained for the samples. The results show, using laminated isogrid instead of conventional one considerably improves the mechanical behavior of the isogrid structures. Moreover, the results depict, the layer's orientation plays an important role in mechanical responses of a grid structure. As shown in the figures, generally the defined structures show their best response at $\theta = 45^\circ$. Investigating the effects of increasing the number of layers shows, there is an optimum value for the number of layers in a laminated isogrid structure. After the optimum value, increasing the number of layers will not be an affordable choice to enhance the mechanical behaviors of the laminated isogrid structures. According to results, despite the identical weight and thickness the mechanical responses of a laminated isogrid structure completely depends on the geometry design.

References

1. Chattopadhyay B, Sinha P and Mukhopadhyay M. Finite element free vibration analysis of eccentrically stiffened composite plates. *Journal of reinforced plastics and composites* 1992; 11(9): 1003–1034.
2. Chen C, Liu W and Chern S. Vibration analysis of stiffened plates. *Computers & structures* 1994; 50(4): 471–480.
3. Prusty BG and Ray C. Free vibration analysis of composite hat-stiffened panels by method of finite elements. *Journal of reinforced plastics and composites* 2004; 23(5): 533–547.
4. Qing G, Qiu J and Liu Y. Free vibration analysis of stiffened laminated plates. *International Journal of Solids and Structures* 2006; 43(6): 1357–1371.
5. Torkamani S, Navazi H, Jafari A et al. Structural similitude in free vibration of orthogonally stiffened cylindrical shells. *Thin-Walled Structures* 2009; 47(11): 1316–1330.
6. Zhou X, Yu D, Shao X et al. Simplified-super-element-method for analyzing free flexural vibration characteristics of periodically stiffened-thin-plate filled with viscoelastic damping material. *Thin-Walled Structures* 2015; 94: 234–252.
7. Belardi V, Fanelli P and Vivio F. Structural analysis and optimization of anisogrid composite lattice cylindrical shells. *Composites Part B: Engineering* 2018; 139: 203–215.
8. Belardi VG, Fanelli P and Vivio F. Design, analysis and optimization of anisogrid composite lattice conical shells. *Composites Part B: Engineering* 2018; 150: 184–195.
9. Frulloni E, Kenny J, Conti P et al. Experimental study and finite element analysis of the elastic instability of composite lattice structures for aeronautic applications. *Composite structures* 2007; 78(4): 519–528.
10. Prusty BG. Free vibration and buckling response of hat-stiffened composite panels under general loading. *International Journal of Mechanical Sciences* 2008; 50(8): 1326–1333.
11. Buragohain M and Velmurugan R. Buckling analysis of composite hexagonal lattice cylindrical shell using smeared

stiffener model. *Defence Science Journal* 2009; 59(3): 230–238.
12. Morozov E, Lopatin A and Nesterov V. Finite-element modelling and buckling analysis of anisogrid composite lattice cylindrical shells. *Composite Structures* 2011; 93(2): 308–323.
13. Shi S, Sun Z, Ren M et al. Buckling resistance of grid-stiffened carbon-fiber thin-shell structures. *Composites Part B: Engineering* 2013; 45(1): 888–896.
14. Ren M, Li T, Huang Q et al. Numerical investigation into the buckling behavior of advanced grid stiffened composite cylindrical shell. *Journal of Reinforced Plastics and Composites* 2014; 33(16): 1508–1519.
15. Weber MJ and Middendorf P. Semi-analytical skin buckling of curved orthotropic grid-stiffened shells. *Composite Structures* 2014; 108: 616–624.
16. Huang L, Sheikh AH, Ng CT et al. An efficient finite element model for buckling analysis of grid stiffened laminated composite plates. *Composite Structures* 2015; 122: 41–50.
17. Kidane S, Li G, Helms J et al. Buckling load analysis of grid stiffened composite cylinders. *Composites Part B: Engineering* 2003; 34(1): 1–9.
18. Ehsani A and Rezaeepazhand J. Vibration and stability of laminated composite orthogrid plates. *Journal of Reinforced Plastics and Composites* 2016; 35(13): 1051–1061.
19. Ehsani A and Rezaeepazhand J. Stacking sequence optimization of laminated composite grid plates for maximum buckling load using genetic algorithm. *International Journal of Mechanical Sciences* 2016; 119: 97–106.
20. Ehsani A and Rezaeepazhand J. Comparison of stiffness and failure behavior of the laminated grid and orthogrid plates. *Journal of Solid Mechanics* 2017; 9(1): 126–137.
21. Ehsani A and Dalir H. Tip angle effect on buckling and deformation of laminated composite anglegrid plates. In *ECCM18 - 18th European Conference on Composite Materials, Athens, Greece*.
22. Ehsani A and Dalir H. Application of laminated composite grids as a reinforcing element of automotive components. In *ASC 33rd Annual Technical Conference -18th US-Japan Conference on Composite Materials*.
23. Naik NK, Sekher YC and Meduri S. Damage in woven-fabric composites subjected to low-velocity impact. *Composites Science and Technology* 2000; 60(5): 731–744.
24. Jones RM. *Mechanics of composite materials*. Taylor and Francis press, 1999.
25. Nemeth MP. A treatise on equivalent-plate stiffnesses for stiffened laminated-composite plates and plate-like lattices. *NASA TP 2011-216882* 2011; .
26. Reddy J. A penalty plate-bending element for the analysis of laminated anisotropic composite plates. *International Journal for numerical methods in Engineering* 1980; 15(8): 1187–1206.
27. Dawe D and Craig T. The vibration and stability of symmetrically-laminated composite rectangular plates subjected to in-plane stresses. *Composite Structures* 1986; 5(4): 281–307.
28. Liew K. Solving the vibration of thick symmetric laminates by reissner/mindlin plate theory and thep-ritz method. *Journal of Sound and Vibration* 1996; 198(3): 343–360.